This article has been accepted for publication in a future issue of this journal, but has not been fully edited. Content may change prior to final publication. Citation information: DOI 10.1109/TMECH.2021.3053562, IEEE/ASME Transactions on Mechatronics

Human-Robot Cooperation Control Based on Trajectory Deformation Algorithm for a Lower Limb Rehabilitation Robot

Jie Zhou, *Student Member, IEEE,* Zhijun Li, *Senior Member, IEEE*
Xianming Li, Xiaoyun Wang, Rong Song, *Senior Member, IEEE*

***Abstract*—Although many studies have certified the advantages of human-robot cooperation control with admittance model (AM), robot compliance and movement smoothness need to be further improved. In this paper, a trajectory deformation algorithm (TDA) is developed as a high-level trajectory planner, which can plan subject's desired trajectory based on interaction force during physical human-robot interaction (pHRI). A low-level proportional-derivative (PD) position controller is selected to ensure the lower limb rehabilitation robot (LLRR) can track the desired trajectory. Then, the validity of TDA is verified through simulation and experiment studies. The energy per unit distance (EPUD) and dimensionless squared jerk (DSJ) are chosen as indicators of robot compliance and movement smoothness, respectively. The experimental results demonstrated that both the EPUD and the DSJ values using TDA are smaller than that using the AM, indicating the TDA can improve robot compliance and movement smoothness. Therefore, it may have great potential in fields involving pHRI, such as robot-aided rehabilitation.**

***Index Terms*—Human-robot cooperation control, lower limb rehabilitation robot, movement smoothness, robot compliance, trajectory deformation algorithm.**

I. Introduction

NEARLy, 2,000,000 people suffer a new stroke each year in China, causing neurological and functional impairments, and hindering patients from performing daily activities [1, 2]. The problem will almost certainly be aggravated by the trend of an aging population, as the incidence of stroke doubles every decade above the age of 55 [3]. Gait training is an important component of stroke rehabilitation, as most stroke survivors have lower limb mobility deficits [4]. Although manually-assisted training can help patients reintegrate into family and society, it requires intensive labor from the physical therapist [5]. Therefore, various types of the lower limb rehabilitation robots (LLRRs), such as Lokomat, Ekso, and Rewalk, have been designed to solve this problem, and many relevant research studies have proven the effectiveness of robot-aided rehabilitation [6-8].

The control strategy of a rehabilitation robot has a significant impact on the rehabilitation effect. The passive control strategy has been used in early rehabilitation robots, which can make patients move along a predefined trajectory under a passive training mode, thereby reducing therapists' workload and extending the training time [9]. Since active participation can induce neural plasticity, active rehabilitation training may promote the recovery of patients [10]. Various active control strategies, such as path control strategy, adaptive seamless assist-as-needed control strategy, and impedance/admittance control strategy, have been proposed based on patients' movement performances to improve patients' active participation. A path control strategy has been proposed for Lokomat, which can keep patients' legs within a "tunnel" using compliant virtual walls, and allow subjects to control their gait timing actively [11]. An adaptive seamless assist-as-needed control strategy based on a robust adaptive controller has been developed for a robotic gait training orthosis, which can learn the disability level of patients in real-time and provide robotic assistance in needed [12]. A torque tracking impedance controller was proposed for a LLRR, and the results showed that the LLRR could provide predefined robotic assistance within an acceptable tracking error range [13]. Jamwal et al. proposed an interactive training paradigm based on impedance control, and four training modes were compared through healthy subject experiments [14]. An admittance control with an inner adaptive robust position controller was proposed for a LLRR with a reference trajectory, which could ensure the robot's compliance and improve tracking accuracy [15]. Besides, an admittance control based on an EMG-driven musculoskeletal model was proposed for an ankle exoskeleton robot without a reference trajectory [16]. Both admittance and impedance control can improve patients' active participation by adjusting the relationship between the position deviation and interaction force/torque [17]. Impedance control can make the robot follow the reference trajectory within a specified tracking error range [13, 14], whereas admittance control can determine the target trajectory according to the patient's active force/torque without any restriction on the reference trajectory [15, 16]. Moreover, due to limited sampling time and sensor

This work was supported by the National Key R&D Program of China Grant No. 2018YFC2001600; the Guangdong Science and Technology Plan Project Grant No. 2017B010110015 and 2017B020210011; the National Natural Science Foundation of China Grant No. U1913601 and U2013601.

J. Zhou, X. Li, and R. Song are with Department of Biomedical Engineering, Sun Yat-Sen University, Guangzhou 510006, China (email:zhouj285@mail2sysu.edu.cn;525514854@qq.com;songrong@mail.sysu.edu.cn)

Z. Li is with Department of Automation, University of Science and Technology of China, Hefei 230026, China (email: zjli@ieee.org).

X. Wang is with the Guangdong Work Injury Rehabilitation Center, Guangzhou 510900, China (e-mail: xiaoyunwang77@hotmail.com)

1083-4435 (c) 2020 IEEE. Personal use is permitted, but republication/redistribution requires IEEE permission. See http://www.ieee.org/publications_standards/publications/rights/index.html for more information.
Authorized licensed use limited to: Carleton University. Downloaded on May 27,2021 at 01:39:09 UTC from IEEE Xplore. Restrictions apply.

This article has been accepted for publication in a future issue of this journal, but has not been fully edited. Content may change prior to final publication. Citation information: DOI 10.1109/TMECH.2021.3053562, IEEE/ASME Transactions on Mechatronics

noise, admittance control is more stable than impedance control under a high impedance interactive environment [17]. Therefore, admittance control, as a typical compliance control strategy, is widely used in rehabilitation robotics.

Admittance control can be explained as follows: a human operator may feel like moving an object with inertial, damping, and stiffness actions from a rest position to a goal position [18]. The admittance model (AM), as a second-order interaction model, needs to adjust the admittance parameters to obtain interactive stability and desired compliance, and this process is troublesome and not intuitive in practical application. Both unknown dynamic contact environment and improper admittance parameters can cause a deviation of the robot from the desired admittance behavior, and it may produce robot oscillating motions of high amplitude and frequency, which can significantly decrease movement smoothness and can even cause safety problems [19, 20]. Besides, although absolute stability can be guaranteed with the passivity framework, the over-conservative admittance parameters may directly increase the energy consumption of the human operator, namely, decrease robot compliance [21]. Since both movement performance and voluntary participation can influence the effectiveness of robot-assisted rehabilitation training [10, 22], interaction performances of admittance control, such as movement smoothness and robot compliance, need to be further improved.

To improve the performance of admittance control, many researchers have conducted extensive research. Although a set of design guidelines were proposed for achieving a high-performance admittance controller, the transitioning stage (from non-contact to contact or contact to non-contact) was neglected in the analysis process [23]. Many variable admittance controllers have been developed to make the robot adapt to a potentially unknown environment and improve the system's interaction performance [24, 25]. A unified impedance and admittance control strategy has been proposed to improve stability and performance properties, which can continuously switch between admittance and impedance controllers [26]. A fractional-order admittance controller has been developed to offer a better trade-off between stability and interaction performance under different contact environments [27]. Many other methods have also been proposed to improve the interaction performance when using admittance/impedance models, such as an impedance adaptation method based on cost function [28] and an impedance learning based on machine learning schemes [29]. However, these methods are challenging to improve robot compliance and movement smoothness simultaneously during physical human-robot interaction (pHRI) under unknown dynamic contact environment, and there are few works of literature to evaluate the interaction performance quantitatively.

In this paper, a trajectory deformation algorithm (TDA) was proposed based on [30], and a human-robot cooperation control strategy with a low-level position controller and a high-level trajectory planner was proposed for a LLRR. The TDA and AM were chosen as trajectory planners to generate the desired trajectory, respectively. Besides, a proportional-derivative (PD) position controller was selected to ensure that the LLRR can track the desired trajectory. To verify the validity of TDA, simulations and experiments were performed, and interaction and tracking performances were analyzed quantitatively. The main contributions of this paper can be summarized as follows: 1) we have improved TDA to ensure that the maximum magnitude of deformation converges with the increase of prediction time. It can make the desired trajectory generated by TDA to remain within a reasonable range when the operator chooses a longer prediction time and ensures the subjects' safety; 2) We have proved that TDA owning more advantages than AM through simulations and experiments. It indicates that TDA can improve robot compliance and movement smoothness under unknown dynamic contact environment.

II. System Description

A. The Designed of LLRR

A new 3-DOF LLRR is manufactured by machining and 3D printing with aluminum and nylon materials, and the virtual and actual prototype are shown in Fig. 1. The length of the aluminum exoskeleton is adjustable to fit subjects of different heights, and different legs (fat and thin) can be fixed on the LLRR using two semicircular leg fixators with Velcro. An actuator module consisting of a brushless flat motor (EC 90 flat, Maxon, Sachseln, Switzerland) and a harmonic reducer (LCD-20-100-C-I, Leader, Jiangsu, China) is developed and used in all joints of the LLRR. Besides, the motor in the actuator module is controlled by a motor driver (1-Q-EC Amplifier DEC Module 50/5, Maxon, Sachseln, Switzerland). The angular position on each joint is sensed using an optical encoder located inside the motor. The interaction force is measured by pressure sensors (L10C-20, Jiuzhi, Shanghai, China) installed on an interaction force measurement device. Moreover, a data acquisition device (NI DAQ, 6341, National Instruments, USA) serves as an interface between the LLRR and a personal computer (PC) with LabVIEW 2013 software.

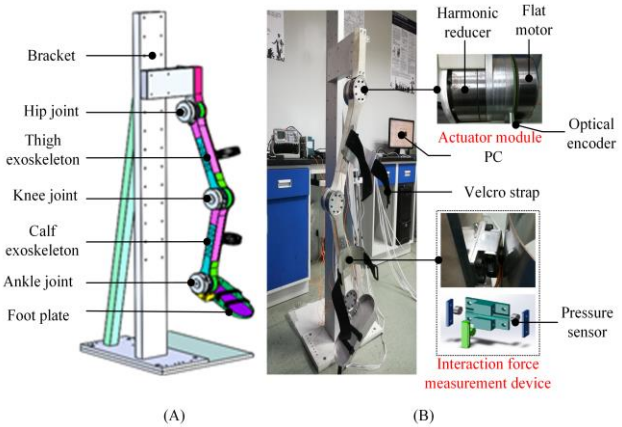

Fig. 1. The hardware configuration of LLRR. (A) is the virtual prototype of LLRR. (B) is the actual prototype of LLRR.

B. System Security

It is essential to protect subjects from injury in experiments, which should be considered during the LLRR system design. Firstly, the maximum range and speed of motion for each joint

1083-4435 (c) 2020 IEEE. Personal use is permitted, but republication/redistribution requires IEEE permission. See http://www.ieee.org/publications_standards/publications/rights/index.html for more information.
Authorized licensed use limited to: Carleton University. Downloaded on May 27,2021 at 01:39:09 UTC from IEEE Xplore. Restrictions apply.

This article has been accepted for publication in a future issue of this journal, but has not been fully edited. Content may change prior to final publication. Citation information: DOI 10.1109/TMECH.2021.3053562, IEEE/ASME Transactions on Mechatronics

is restricted within a normal range [31]. Once the control system detects that the actual position or angular velocity exceeds the corresponding limits during the experiment, it will stop the system and immediately shut down the LLRR. Secondly, if the subject feels uncomfortable, the supervisor can shut down the LLRR through an emergency shutdown button. Thirdly, if the former two protection methods fail, the limitation of mechanical structure on the range of motion joint angles will play a final protective role for subjects.

III. METHOD

A. Trajectory Deformation Algorithm

The human motion intention in a human-robot cooperative task is usually defined as the desired trajectory [18, 32]. In that regard, pHRI affects not only the current state of the robot but also its future behavior. Therefore, a trajectory planner should be able to generate smooth current and future trajectories continuously. To explore this concept more formally, we introduce some notations, and a diagram of the current trajectory deformation is shown in Fig. 2.

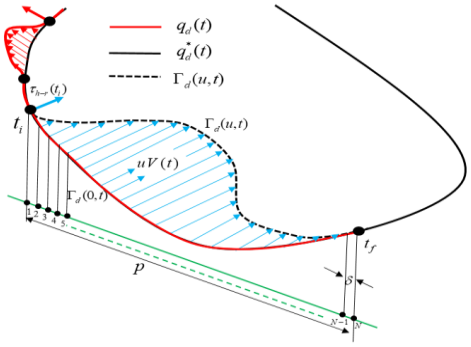

Fig. 2. Diagram of the current trajectory deformation.

We define $q_d^*(t)$ as the reference trajectory, $q_d(t)$ as the desired trajectory, δ as the sample period, N as the number of waypoints, u as the deformation factor, p as the prediction time, $V(t)$ as the vector field function, t_i and t_f as the start and end time of the current trajectory deformation, respectively. Besides, $\Gamma_d(u,t)$ is defined as a deformation curve function, which can yield different smooth deformation curves over the time interval $t \in [t_i, t_f]$ by adjusting deformation factor u. The desired trajectory between t_i and t_f, can be defined as follows:

$$\Gamma_d(0,t)=\left[q_d(t_i), q_d(t_i+\delta), \cdots, q_d(t_i+(N-2)\delta), q_d^*(t_f)\right] \quad (1)$$

The deformation curve function $\Gamma_d(u,t)$ in the current iteration can be obtained through a vector field function $V(t)$ and a deformation factor u based on the desired trajectory $\Gamma_d(0,t)$ between t_i and t_f. Therefore, once pHRI occurs at an arbitrary time t_i, the desired trajectory $\Gamma_d(0,t)$ between t_i and t_f can change smoothly in response to an interaction torque $\tau_{h-r}(t_i)$ within the prediction time p. If the deformation curve function $\Gamma_d(u,t)$ can be obtained, the desired trajectory $q_d(t)$ will be updated next, such that $q_d(t) = \Gamma_d(u,t), t \in [t_i, t_f]$. Then, the desired trajectory between $t_i+\delta$ and $t_f+\delta$ can be updated as follows:

$$\Gamma_d(0,t)=\left[q_d(t_i+\delta), q_d(t_i+2\delta), \cdots, q_d(t_f), q_d^*(t_f+\delta)\right] \quad (2)$$

It is worth mentioning that, although we focus on the current trajectory deformation, the desired trajectory in the entire human-robot interaction process is continuously generated in response to the interaction torque through an iterative process. Moreover, the prediction time p can ensure the deformation curve function $\Gamma_d(u,t)$ return to the reference trajectory $q_d^*(t)$ in the absence of additional human-robot interaction.

Analogously to what is done in [30], we can propose the final equation of TDA as follows, and the specific derivation process of TDA is provided in appendix.

$$\begin{cases} \Gamma_d(u,t) = \Gamma_d(0,t) + uV(t), \quad t \in [t_i, t_f] \\ V(t) = \delta H \tau_{h-r}(t_i) \\ H = \dfrac{W\beta}{(p+\delta)\|W\|} \end{cases} \quad (3)$$

where

$$\tau_{h-r}(t_i) = Lf(t_i) \quad (4)$$

$$W = (I - (Z^T Z)^{-1} C^T (C(Z^T Z)^{-1} C^T)^{-1} C)(Z^T Z)^{-1}, I \in R^{N \times N} \quad (5)$$

$$N = \frac{p}{\delta} + 1 \quad (6)$$

where L and $f(t_i)$ are the lever arm of the interaction force and interaction force at the current time t_i respectively, $Z \in R^{(N+3)\times N}$ is a finite differencing matrix, $C \in R^{4\times N}$ is a constraint matrix of vector field function, $I \in R^{N\times N}$ is an identity matrix, $\beta \in R^N$ is the prediction vector of the interaction torque.

We define H as a motor primitive function, and it determines the shape of the vector field function $V(t)$. Let $\beta = \vec{1} \in R^N$ and the shape of the motor primitive function with respect to N can be seen in Fig. 3.

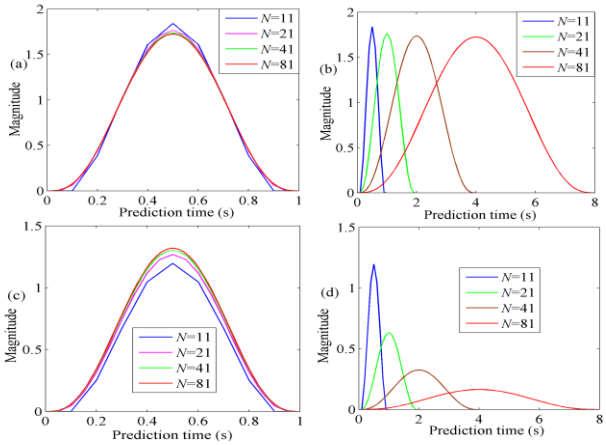

Fig. 3. The shape of the motor primitive function under different parameters. (a) and (b) are the results for the motor primitive function in [30]. (c) and (d) are the results for the motor primitive function in this study.

1083-4435 (c) 2020 IEEE. Personal use is permitted, but republication/redistribution requires IEEE permission. See http://www.ieee.org/publications_standards/publications/rights/index.html for more information.
Authorized licensed use limited to: Carleton University. Downloaded on May 27,2021 at 01:39:09 UTC from IEEE Xplore. Restrictions apply.

This article has been accepted for publication in a future issue of this journal, but has not been fully edited. Content may change prior to final publication. Citation information: DOI 10.1109/TMECH.2021.3053562, IEEE/ASME Transactions on Mechatronics

From Figs. 3(a) and (c), both motor primitive functions of TDA converge to an ideal shape with an increase of N when prediction time is set to 1 s. As shown in Figs. 3(b) and (d), the maximum magnitude of motor primitive function proposed in this study slowly converges to 0 with the increase of N when the sample period is set to 0.1 s, whereas the maximum magnitude of motor primitive function proposed in [30] remains near-constant value. The reason is that the increase of N caused by the decrease of sampling period will make the final curve of motion primitive function converge to the bell-shaped curve $H = \frac{W\beta}{p\|W\|}$, and the increase of N caused by the increase of prediction time has a significant impact on the amplitude of the bell-shaped curve, which will eventually make the amplitude of the bell-shaped curve converge to 0.

B. Admittance Model

Impedance/admittance control strategy is widely used in research involving pHRI, which correlates position tracking errors to forces, according to a mass-spring-damper relationship [33]. Although the reference trajectory can be set before the experiment, the desired trajectory is determined online by the subject when using AM. If the reference trajectory of the LLRR is defined as $q_d^*(t)$, AM can be formulated as follows:

$$M(\ddot{q}_d(t)-\ddot{q}_d^*(t))+B(\dot{q}_d(t)-\dot{q}_d^*(t))+K(q_d(t)-q_d^*(t))=\tau_{h-r}(t) \quad (7)$$

where M, B and K are the desired inertia, damping and stiffness, respectively. $q_d(t)$, $\dot{q}_d(t)$ and $\ddot{q}_d(t)$ are the desired trajectory, desired angular velocity and desired angular acceleration of the LLRR, respectively. $q_d^*(t)$, $\dot{q}_d^*(t)$ and $\ddot{q}_d^*(t)$ are the reference trajectory, reference angular velocity, reference angular acceleration of the LLRR, respectively. $\tau_{h-r}(t)$ is an interaction torque between the subject and the LLRR.

C. Control Strategy of LLRR

A human-robot cooperation control strategy is proposed, and the corresponding control flow chart is shown in Fig. 4. The control strategy consists of a high-level trajectory planner and a low-level position controller. The TDA and AM are set as the trajectory planners, respectively, and a simple PD position controller is selected to ensure that the LLRR can complete the trajectory tracking task.

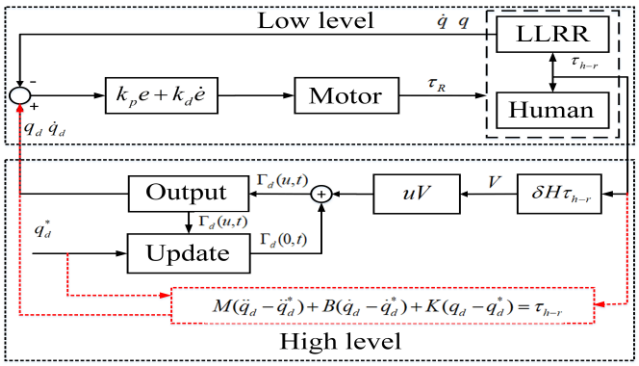

Fig. 4. Control flow chart of the LLRR based on TDA or AM.

D. Evaluation Method

The dimensionless squared jerk (DSJ) [34] and the normalized root mean square deviation (NRMSD) are utilized to compare the performances of the LLRR using the different trajectory planners. The DSJ and the NRMSD can be expressed as follows:

$$DSJ = \int_{t_a}^{t_b} \dddot{\theta}(t)^2 dt \frac{(t_b - t_a)^5}{A^2} \quad (8)$$

$$NRMSD = \frac{\sqrt{\frac{\sum_{j=1}^{n} e^2(t_j)}{n}}}{\max(q_d) - \min(q_d)} \quad (9)$$

where A is the maximum amplitude of trajectory, $\dddot{\theta}(t)$ is the third derivative of the trajectory (desired trajectory or tracking trajectory), the time parameters t_a and t_b are the start and end of trajectory respectively, $j = 1, 2, 3, \cdots, n$ is the sample number, $e(t_j)$ is the error between the desired trajectory and tracking trajectory at the time t_j, $\max(q_d)$ and $\min(q_d)$ are the maximum and minimum desired position respectively. A smaller DSJ value indicates a smoother movement, and a smaller NRMSD value indicates a higher tracking accuracy.

With robot compliance improvement, the subject can freely move the robot with less interaction force. Therefore, the energy per unit distance (EPUD) can be chosen as an index of robot compliance [35]. Referring to this literature, the EPUD is proposed as follows:

$$EPUD = \frac{\sum_{j=1}^{n} \left| \tau_{h-r}(t_j) \Delta d(t_j) \right|}{\sum_{j=1}^{n} \left| \Delta d(t_j) \right|} \quad (10)$$

where $\Delta d(t_j)$ is the deviation between the reference trajectory and desired trajectory at the time t_j; $\tau_{h-r}(t_j)$ is an interaction torque between the subject and the LLRR at the time t_j. A smaller EPUD value indicates higher robot compliance.

IV. Simulations And Experiments

In this section, two types of trajectory planners and corresponding human-robot cooperative control strategies are simulated in MATLAB (2014a). Then, experiments are performed on five healthy subjects using the proposed control strategies, and experimental results are presented.

A. Simulation Studies

1) Simulation of TDA and AM

To study the properties of AM and TDA, we perform simulation experiments in MATLAB (2014a). The interaction force is defined as $f(t)$, and it can be formulated as follows:

$$f(t) = \begin{cases} 1, if\ 2 \le t \le 5 \\ 0, otherwise \end{cases} \quad (11)$$

We set the reference trajectory q_d^* as zero. The other basic parameters are set as follows:

$$L = 1, \beta = \vec{1} \in R^N \quad (12)$$

1083-4435 (c) 2020 IEEE. Personal use is permitted, but republication/redistribution requires IEEE permission. See http://www.ieee.org/publications_standards/publications/rights/index.html for more information.
Authorized licensed use limited to: Carleton University. Downloaded on May 27,2021 at 01:39:09 UTC from IEEE Xplore. Restrictions apply.

This article has been accepted for publication in a future issue of this journal, but has not been fully edited. Content may change prior to final publication. Citation information: DOI 10.1109/TMECH.2021.3053562, IEEE/ASME Transactions on Mechatronics

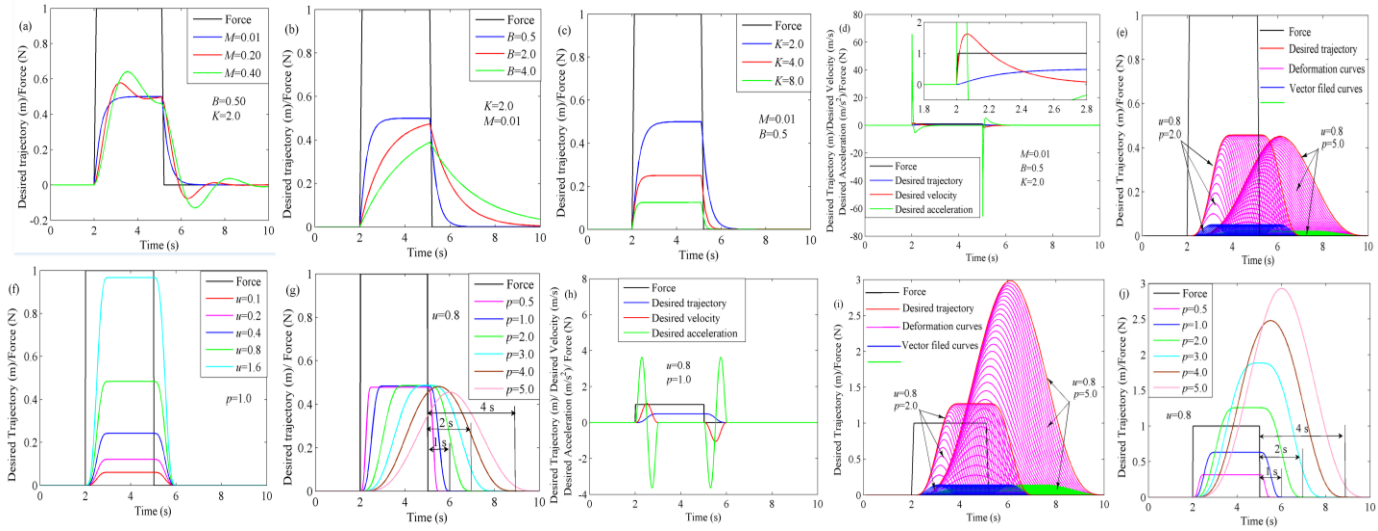

Fig. 5. Simulation results for different trajectory planners. (a), (b), (c), and (d) are the results for AM. (e), (f), (g), and (h) are the results for TDA proposed in this study. (i) and (j) are the results for TDA proposed in [30].

The desired trajectories generated by AM and TDA are shown in Fig. 5. From Figs. 5(a), (b), and (c), the amplitude and convergence time of the desired trajectory generated by AM are affected by inertia, damping, and stiffness simultaneously, and improper inertia parameters may cause the desired trajectory to oscillate.

Figs.5 (e) and (i) show the generation process of the desired trajectory by TDA. Firstly, the vector field curves (in green or blue) at different times are generated sequentially, based on the interaction torque and motion primitive function. Then, the deformation curves (in magenta) at different times are produced through the linear combination of different vector field curves. Finally, once we obtain the deformation curves, the desired trajectory (in red) can be updated online. As shown in Fig. 5(f), the desired trajectory raises rapidly with an increase of the deformation factor when the prediction time is set to a constant value (1 s). This means that the robot compliance can be easily adjusted through a single parameter within a prediction time window. From Fig. 5(j), the maximum magnitude of the desired trajectory increases rapidly with the extension of the prediction time window when using TDA proposed in [30]. However, the maximum magnitude of the desired trajectory quickly reaches its maximum, and then gradually decreases with the increase of prediction time when using TDA proposed in this study, as shown in Fig. 5(g). The reason is that the maximum magnitude of motor primitive function proposed in this study slowly converges to 0 with the increase of waypoints' number, which will lead to the fast convergence of vector field curves' amplitude, as shown in Fig.5 (e). This result indicates that the maximum magnitude of the deformation is convergent, which can ensure that the desired trajectory remains within a reasonable range when the operator chooses a longer prediction time. Besides, it is worth mentioning that the dynamics characteristics of TDA are determined by the prediction time, and the dynamic response speed decreases with the increase of prediction time.

Moreover, compared with the desired trajectories generated by AM, we can find that TDA can ensure a smoother transition of the desired trajectory during the transitioning stage (from non-contact to contact or contact to non-contact). From Fig. 5(d), the desired acceleration, desired velocity, and desired trajectory generated by AM are unsmooth during the transitioning stage. Fig. 5(h) shows that the desired acceleration, desired velocity, and desired trajectory generated by TDA are smooth enough, and bell-shaped velocity curves can be obtained at the beginning and end contacts.

2) Simulation of Control Strategy

Simulations of human-robot cooperation control strategies are carried in MATLAB (2014a) to explore the impacts of unstable interactions on different control strategies' performances. The interaction force will be defined as follows to simulate an unknown dynamic contact environment in each simulation.

$$f_{hip}(t)=\begin{cases}100, [0.5,1.5]\cup[4,5.5]\\ -100, [2,3.5]\cup[6,7.5]\\ 0, otherwise\end{cases} \tag{13}$$

$$f_{knee}(t)=\begin{cases}100, [1,2.5]\cup[5,6.5]\\ -100, [3,4.5]\cup[7,8.5]\\ 0, otherwise\end{cases} \tag{14}$$

The kinetic equation of a LLRR has been deduced in previous studies [36], and the relevant structural parameters and control parameters are shown in Table I and Table II. For simplicity, the lower limb's mass and inertia parameters are set to be the same as those of LLRR. The simulation time and sample time are set to 10 s and 0.01 s, respectively. In that regard, PD position controller with TDA and PD position controller with AM are abbreviated as PD-TDA and PD-AM, respectively. The desired trajectory, reference trajectory, and tracking trajectory are abbreviated as DT, RT, and TT, respectively. Moreover, we choose a subject's gait trajectory captured by a motion capture system as the reference trajectory. A sinusoidal function fitting is necessary to obtain a sufficiently smooth periodic reference trajectory.

As shown in Figs. 6 (a), 6 (b), 7 (a) and 7 (b), the trajectory planner (TDA or AM) can continuously generate a subject's desired trajectory when pHRI occurs, and the desired trajectory

1083-4435 (c) 2020 IEEE. Personal use is permitted, but republication/redistribution requires IEEE permission. See http://www.ieee.org/publications_standards/publications/rights/index.html for more information.
Authorized licensed use limited to: Carleton University. Downloaded on May 27,2021 at 01:39:09 UTC from IEEE Xplore. Restrictions apply.

This article has been accepted for publication in a future issue of this journal, but has not been fully edited. Content may change prior to final publication. Citation information: DOI 10.1109/TMECH.2021.3053562, IEEE/ASME Transactions on Mechatronics

TABLE III
RESULTS OF SIMULATIONS

Control Strategy	Interaction Performance				Tracking Performance			
	DSJ of Desired Trajectory		EPUD		DSJ of Tracking Trajectory		NRMSD (%)	
	Hip	Knee	Hip	Knee	Hip	Knee	Hip	Knee
PD-AM	4.0926×10^{13}	1.2866×10^{13}	16.0792	16.5357	1.5237×10^{13}	1.3525×10^{13}	0.61	0.31
PD-TDA	3.5983×10^{9}	1.1319×10^{9}	13.5301	14.1838	9.0993×10^{12}	9.0419×10^{12}	0.67	0.32

TABLE I
STRUCTURAL PARAMETERS OF LLRR

Symbol	Description	Thigh (i=1)	Calf (i=2)
m_i (kg)	The mass of exoskeleton	2.582	3.192
l_i (m)	The lengths of exoskeleton	0.390	0.464
d_i (m)	The length from the center of mass to the revolute joint	0.328	0.355
I_i (kg m^2)	The inertias of exoskeleton	0.307	0.446

TABLE II
CONTROL PARAMETERS OF CONTROL STRATEGY

Symbol	Description	Value	Units
k_p	PD parameter	$diag\{4000, 4000\}$	-
k_d	PD parameter	$diag\{90, 90\}$	-
M	Inertia	$diag\{0.2, 0.2\}$	Nm/(rad·s^2)
B	Damping	$diag\{30, 30\}$	Nm/(rad·s)
K	Stiffness	$diag\{100, 100\}$	Nm/rad
L	Lever arm	0.2	m
β	Prediction vector	$\vec{1} \in R^N$	-
p	Prediction time	1	s
δ	Sample period	0.01	s
u	deformation factor	$diag\{0.0125, 0.0125\}$	-

gradually converges back to the reference trajectory once pHRI stops. It is worth mentioning that the convergence time of the desired trajectory generated by TDA (1 s) is shorter than that of AM (more than 1 s), and the tracking trajectory can follow the desired trajectory well. Figs.6(c) and 7(c) show that the control torque of the hip and knee joint when using AM shows more obvious impact characteristics than that using TDA. As shown in Figs. 6(d) and 7(d), the desired angular velocity and acceleration generated by TDA are smoother than that generated by AM.

Table III shows quantitative evaluation results for PD-AM and PD-TDA. In terms of the interaction performance, DSJ values of the hip and knee joint trajectories generated by TDA are 99.99% and 99.99% less than those created by AM, respectively. Moreover, EPUD values of the hip and knee joint using TDA are reduced by 15.85 % and 14.22%, respectively, compared to those using AM. In terms of tracking performance, DSJ values of the hip and knee joint tracking trajectories using PD-TDA are 40.28% and 33.15% less than those using PD-AM, respectively. This result indicates that TDA can improve the robot compliance and movement smoothness, even if the convergence time of the desired trajectory is shorter than that of AM. Besides, compared to PD-AM, NRMSD values of the hip and knee joints using PD-TDA are increased by 9.84% and 3.23%, respectively.

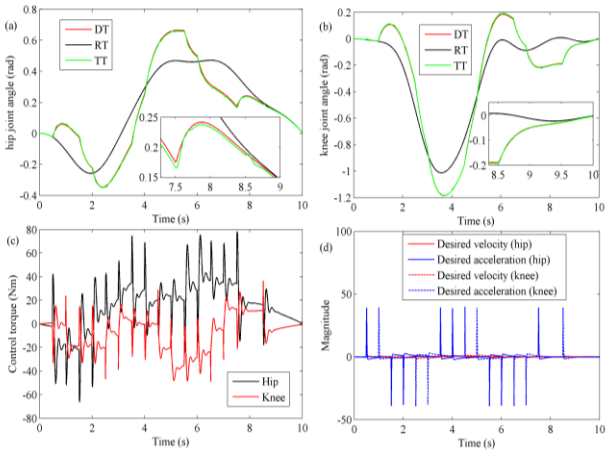

Fig. 6. Simulation results for PD-AM.

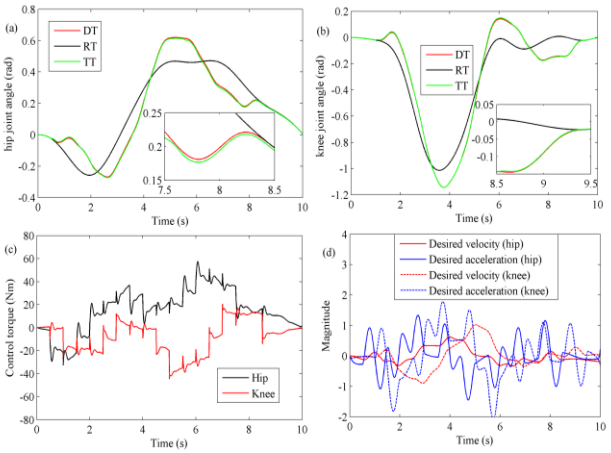

Fig. 7. Simulation results for PD-TDA

B. *Experimental Studies*

We carried out the experiments for the proposed human-robot cooperation control strategies on five healthy subjects (two males, three females, mean age: 26.4±2.3years). All subjects had written informed consent before participating in the experiment, and ethical approval of our study was granted by Guangdong Work Injury Rehabilitation Center. The sample period was set to 0.1 s to improve computational efficiency, other parameters of TDA and AM were set the same as in the simulation process, and PD parameters were set according to the experimental experiences and actual needs. Doing simple training for each subject before the experiment was necessary, and it can help alleviate the influence of initial skill differences on experimental results. In the experimental process, each subject was required to apply active torque to simulate an unknown dynamic contact environment and execute five trials for each human-robot cooperation control strategy. We calculated the average interaction performance

1083-4435 (c) 2020 IEEE. Personal use is permitted, but republication/redistribution requires IEEE permission. See http://www.ieee.org/publications_standards/publications/rights/index.html for more information.
Authorized licensed use limited to: Carleton University. Downloaded on May 27,2021 at 01:39:09 UTC from IEEE Xplore. Restrictions apply.

This article has been accepted for publication in a future issue of this journal, but has not been fully edited. Content may change prior to final publication. Citation information: DOI 10.1109/TMECH.2021.3053562, IEEE/ASME Transactions on Mechatronics

and average tracking performance of each subject, and the paired t-test was adopted to test the effects of the human-robot cooperation control strategy type statistically.

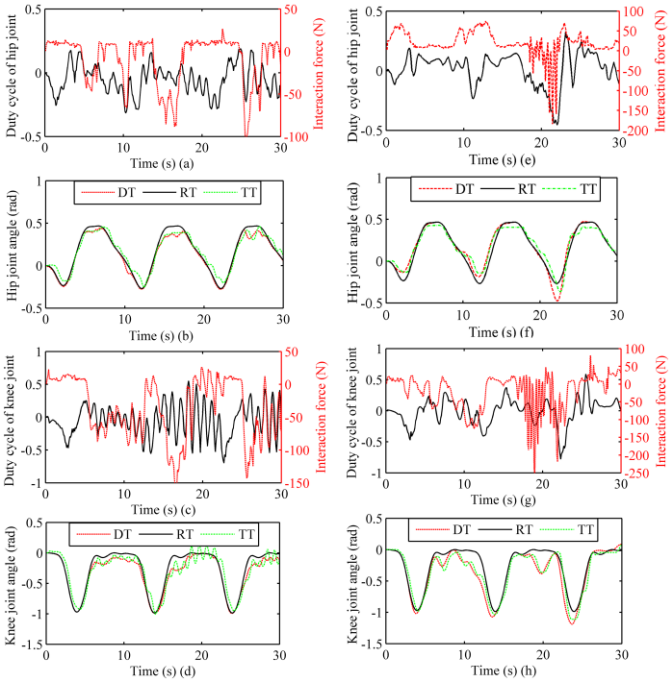

Fig. 8. Experimental results of one subject. (a), (b), (c), and (d) are the experimental results for PD-AM. (e), (f), (g), and (h) are the experimental results for PD-TDA.

The results of PD-AM and PD-TDA are shown in Fig.8. From Figs. 8(b), (d), (f), and (h), compared to TDA, AM has difficulty in guaranteeing the movement smoothness under unknown dynamic contact environment, and the deviations between the reference trajectory and the desired trajectory of the hip and knee joint are smaller when pHRI occurs. From Figs. 8 (e) and (g), the duty cycle curves of the hip and knee actuator using TDA show no violent oscillations during the entire experiment even when the interaction force is altered abruptly. Although the amplitude of the interaction force using AM is smaller (such as Fig. 8(c), 6-12 s) than that of TDA (such as Fig. 8(g), 16-22 s), the oscillations of the duty cycle curve is more significant.

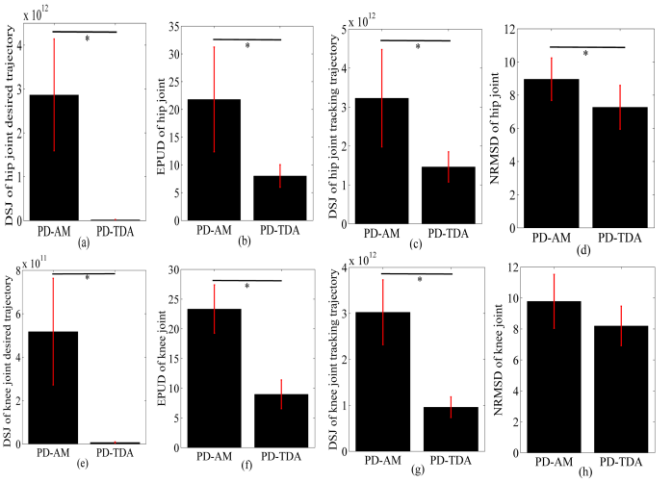

Fig. 9. Quantitative analysis results of experimental data. Each graph shows the mean of each index of all subjects. The error bar indicates the standard deviation of each index, and the asterisk (*) indicates $p < 0.05$.

The quantitative analysis results are summarized in Fig. 9. In terms of the interaction performance, as shown in Figs. 9(a), (b) (e), and (f), DSJ means of the knee and hip joint desired trajectories generated by TDA are 99.47% and 98.63% less than those created by AM, respectively. Furthermore, EPUD means of the knee and hip joints using TDA are reduced by 63.25% and 61.52%, respectively, compared to those using AM. It should be noted that the reduction of DSJ and EPUD is statistically significant. In terms of tracking performance, as shown in Figs. 9(c), (d), (g), and (h), DSJ means of the hip and knee joint tracking trajectories using PD-TDA are 54.68% and 68.28% less than those using PD-AM, respectively. We conclude that the reduction of DSJ is statistically significant when using PD-TDA. Compared to PD-AM, NRMSD means of the hip and knee joints using PD-TDA are reduced by 18.86% and 16.21%, respectively. However, only the reduction of NRMSD in the hip joint is determined to be statistically significant.

V. Discussion

A. Improvement in Movement Smoothness

The smoothness of the kinematic control of the LLRR is a crucial factor in facilitating pHRI and increasing the rehabilitation training effect [22]. However, an unknown dynamic contact environment may jeopardize the stability of the control system, which can lead to significantly decreased movement smoothness [37]. In this study, the human-robot cooperation control strategy with AM has difficulty in guaranteeing the movement smoothness under an unknown dynamic contact environment. Although we can improve the movement smoothness by designing and adjusting admittance parameters, the process needs to balance movement smoothness and operators' effort. Furthermore, there are no specific guidelines for designing and adjusting admittance parameters, especially involving the transitioning stage [23], [38]. Compared with AM, TDA shows significant improvement in movement smoothness even under an unstable contact environment. The reason for the decrease of DSJ value is that TDA considers more motion behavior characteristics of the human body, such as the minimal jerk criterion and motion superposition mechanism. TDA can make a trade-off between the interaction force and trajectory deviation during pHRI, and it is similar to the human body that interacts with unknown environments [39]. The desired trajectory at different times is produced through the linear combination of different vector field curves, and the iterative generation process of TDA is similar to the motion superposition mechanism of human motion planning [40, 41]. Moreover, the cost function of TDA contains movement smoothness sub-item, and velocity curves at the beginning and end contacts are both bell-shaped profile. These show that TDA satisfies the minimal jerk criterion [42].

B. Improvement in Robot Compliance

There is an increasing demand for robot compliance in human-robot cooperation tasks, meaning that robots should allow human operators to direct the robot's motion with a

1083-4435 (c) 2020 IEEE. Personal use is permitted, but republication/redistribution requires IEEE permission. See http://www.ieee.org/publications_standards/publications/rights/index.html for more information.
Authorized licensed use limited to: Carleton University. Downloaded on May 27,2021 at 01:39:09 UTC from IEEE Xplore. Restrictions apply.

This article has been accepted for publication in a future issue of this journal, but has not been fully edited. Content may change prior to final publication. Citation information: DOI 10.1109/TMECH.2021.3053562, IEEE/ASME Transactions on Mechatronics

smaller force [43]. Patients can be allowed to move with greater degrees of freedom when robot compliance is increased, which can improve the patient's active participation during active rehabilitation training [17]. In this study, the overall behavior of TDA is that it enforces no deviations from a reference trajectory when the subject does not want to change his motion, and allows for large deviations when the human subject wishes to move in his/her desired way. In addition, EPUD value using TDA is less than that using AM. The reason is that the work done by the trajectory deformation to the human is considered in the cost function of TDA, and the energy consumption of the interaction can be minimized at any time. Furthermore, TDA contains a specific characteristic that can predict the subject's behavior. This means that the LLRR knows the future trajectory of the subject, and can provide more effective assistance based on this prior information. It is worth mentioning that, compared to [30], TDA can ensure the desired trajectory within a reasonable range when the operator chooses a longer prediction time, which can prevent patients from secondary injury during rehabilitation training. The reason is that a new motion primitive function is designed in this study, which can make the maximum magnitude of deformation convergent with the increase of the prediction time.

C. Parameters adjustment of TDA

The parameter adjustment of TDA is more intuitive and simpler than that of AM because the coupling effect of parameters on interaction performance is reduced. In this study, TDA has four adjustable parameters: prediction vector, sampling period, prediction time, and deformation factor. The prediction vector can be used to modulate the final curve shape of motion primitive function, and the symmetrical bell-shaped curve can be selected in most cases, that is, the prediction vector is set to $\vec{1} \in R^N$. The sampling period is usually set to be consistent with that of the control system, and an integer scale factor should be used to improve the calculation efficiency when the sampling frequency of the control system is high [30]. The robot compliance is mainly determined by the deformation factor, which is similar to the reciprocal of the stiffness. A smaller interaction torque can generate a more considerable trajectory deviation when the deformation factor is set to a large value. Conversely, as the set value of the deformation factor approaches zero, it becomes challenging to create a trajectory deviation. Similar to [14], the switch from active training mode to passive training mode can be realized by setting the deformation factor to 0. The dynamic characteristics of human-robot interaction are mainly determined by the prediction time, and slowing down the robot's dynamic response by increasing the prediction time can improve the movement smoothness. It is worth noting that the increase of prediction time will increase the control system's calculation amount. Therefore, the dynamics characteristics of human-robot interaction and computational efficiency should be balanced in practical application.

D. Future Applications and Limitations

Impaired walking function after stroke presents with various symptoms, such as lower limb adductor spasticity, limb shaking, tremors, and a combination of these symptoms, greatly contributing to functional disability [44-46]. The limbs of the patients can be regarded as an unknown dynamic contact environment because of these symptoms. TDA can make the trajectory of rehabilitation training more natural and smoother under this unknown dynamic contact environment, which will further improve the rehabilitation effect. Moreover, the improvement in robot compliance when using TDA can increase the ability of the LLRR to follow the patient's movement without applying large resistive force, which can encourage patients to participate in training actively and avoid secondary injury caused by excessive interaction force. Additionally, compared to the damping and inertia characteristics, the stiffness characteristics of limbs are easier to obtain using the index of muscle co-contractions [47] and electromyography-driven-musculoskeletal model [48], and the reciprocal of the stiffness can be used as a deformation factor of TDA. Therefore, compared with AM, TDA may be more suitable for robot-aided rehabilitation.

However, there are several limitations in this study that should be addressed in the future. Firstly, the subjects in the comparative experiment are physically healthy, and patients suffering from neurological diseases are not included in this study. Secondly, since the active torque exerted by the subjects is directly applied to the LLRR as the driving torque, the tracking trajectory's smoothness is far less than that of the desired trajectory. In future research, a more robust position controller should be adopted, and patient-based experiments will be conducted to verify the clinical effectiveness of human-robot cooperation control based on TDA during active rehabilitation training.

VI. Conclusion

In this study, a new LLRR was designed, and a TDA was proposed to improve robot compliance and movement smoothness. To verify the effectiveness of TDA, simulations and experimental studies were conducted, and quantitative analysis of the movement smoothness and robot compliance was also performed. The results of the simulations and experiments have been provided to verify that TDA can improve the robot compliance and movement smoothness. Therefore, TDA has the potential to be used in active rehabilitation of patients with motor disorders, and in other fields involving pHRI.

Appendix

1) Problem Statement

The expression of arbitrary deformation curve function $\Gamma_d(u,t)$ between t_i and t_f can be defined as follows:

$$\Gamma_d(u,t) = \Gamma_d(0,t) + uV(t), \forall t \in [t_i, t_f] \tag{15}$$

where t_i and t_f are the start and end time of the current trajectory deformation, $\Gamma_d(0,t)$ is the desired trajectory between t_i and t_f, u is a deformation factor, $V(t)$ is a vector field

1083-4435 (c) 2020 IEEE. Personal use is permitted, but republication/redistribution requires IEEE permission. See http://www.ieee.org/publications_standards/publications/rights/index.html for more information.
Authorized licensed use limited to: Carleton University. Downloaded on May 27,2021 at 01:39:09 UTC from IEEE Xplore. Restrictions apply.

This article has been accepted for publication in a future issue of this journal, but has not been fully edited. Content may change prior to final publication. Citation information: DOI 10.1109/TMECH.2021.3053562, IEEE/ASME Transactions on Mechatronics

function. Besides, vector field function satisfies the following formula

$$V(t) = \partial_u \Gamma_d(u,t), \forall t \in [t_i, t_f] \tag{16}$$

To ensure the continuity of the desired trajectory, we constrain the vector field function as follows:

$$V(t_i) = V(t_f) = 0 \tag{17}$$

$$\dot{V}(t_i) = \dot{V}(t_f) = 0 \tag{18}$$

The deformation curve function can be obtained through a vector field function and a deformation factor based on the desired trajectory. However, there are many choices of vector field function that satisfy these constraints when deformation factor is set to a positive constant. Thus, the critical issue is to find the "best" vector field function.

2) Cost Function of Trajectory Deformation

The desired trajectory $\Gamma_d(0,t)$ between t_i and t_f can be evenly and arbitrarily divided into small segments, and the number of waypoints N is given by

$$N = \frac{p}{\delta} + 1 \tag{19}$$

where δ is the sample period, p is the prediction time. Thus, desired trajectory $\Gamma_d(0,t)$ and deformation curve function $\Gamma_d(u,t)$ between t_i and t_f can be discretized as follows:

$$\gamma = [q_d(t_i), q_d(t_i+\delta), \cdots, q_d(t_i+(N-2)\delta), q_d^*(t_f)]^T \tag{20}$$

$$\tilde{\gamma} = [\Gamma_d(u,t_i), \Gamma_d(u,t_i+\delta), \cdots, \Gamma_d(u,t_i+(N-2)\delta), \Gamma_d(u,t_f)]^T \tag{21}$$

where $q_d^*(t)$ and $q_d(t)$ are the reference trajectory and the desired trajectory at any time t, respectively. It is worth noting that the initialization desired trajectory $\Gamma_d(0,t), \forall t \in [0, t_f]$ can be expressed as follows:

$$\gamma = [q_d^*(0), q_d^*(\delta), \cdots, q_d^*((N-2)\delta), q_d^*(t_f)]^T \tag{22}$$

we define $\hat{\tau}_{h-r} \in R^N$ as the interaction torque vector, and it can be written as follows:

$$\hat{\tau}_{h-r} = [\tau_{h-r}(t_i), \tau_{h-r}(t_i+\delta), \cdots, \tau_{h-r}(t_i+(N-2)\delta), \tau_{h-r}(t_f)]^T \tag{23}$$

$$\tau_{h-r}(t_i) = Lf(t_i) \tag{24}$$

where $\tau_{h-r}(t_i)$ is the interaction torque at the current time t_i, $f(t_i)$ is the interaction force at the current time t_i, L is the lever arm of the interaction force. Since the future interaction torque values at other discrete waypoints are unknown, an online prediction of the interaction torque is needed. The interaction torque vector can be defined as follows:

$$\hat{\tau}_{h-r} = \beta \tau_{h-r}(t_i) = L\beta f(t_i) \tag{25}$$

where $\beta \in R^N$ is the prediction vector of the interaction torque. To obtain the optimal vector field function, similar to [30], the cost function using the waypoints can be defined as follows:

$$J(\tilde{\gamma}) = (\tilde{\gamma}-\gamma)^T(-\hat{\tau}_{h-r}) + \frac{1}{2\alpha u}(\tilde{\gamma}-\gamma)^T(Z^TZ)(\tilde{\gamma}-\gamma) \tag{26}$$

where α and u are positive constants, Z is a finite differencing matrix as follows:

$$Z = \begin{bmatrix} 1 & 0 & 0 & \cdots & 0 \\ -3 & 1 & 0 & \cdots & 0 \\ 3 & -3 & 1 & \cdots & 0 \\ -1 & 3 & -3 & \cdots & 0 \\ 0 & -1 & 3 & \cdots & 0 \\ 0 & 0 & -1 & \cdots & 0 \\ \vdots & \vdots & \vdots & \ddots & \vdots \\ 0 & 0 & 0 & \cdots & 1 \\ 0 & 0 & 0 & \cdots & -3 \\ 0 & 0 & 0 & \cdots & 3 \\ 0 & 0 & 0 & \cdots & -1 \end{bmatrix}, Z \in R^{(N+3)\times N}$$

The first term denotes the work done by the trajectory deformation to the human. In the second term, we use the finite differencing matrix to ensure that the deformation trajectory is natural and smooth.

3) Constrained Optimization

According to the definition of a derivative, and the equation (15), the constraint equations (17) and (18) can be rewritten as follows:

$$\begin{cases} \tilde{\gamma}(1) - \gamma(1) = V(t_i) = 0 \\ \tilde{\gamma}(2) - \gamma(2) = V(t_i+\delta) = 0 \\ \tilde{\gamma}(N-1) - \gamma(N-1) = V(t_i+(N-2)\delta) = 0 \\ \tilde{\gamma}(N) - \gamma(N) = V(t_f) = 0 \end{cases} \tag{27}$$

The above constraint equations can be rewritten and extended to the following matrix form

$$C(\tilde{\gamma}-\gamma) = CV = 0 \tag{28}$$

where

$$C = \begin{bmatrix} 1 & 0 & 0 & \cdots & 0 & 0 & 0 \\ 0 & 1 & 0 & \cdots & 0 & 0 & 0 \\ 0 & 0 & 0 & \cdots & 0 & 1 & 0 \\ 0 & 0 & 0 & \cdots & 0 & 0 & 1 \end{bmatrix}, C \in R^{4\times N}$$

Combining equation (26) and equation (28), we now propose our optimization problem

$$\min \ J(\tilde{\gamma})$$

$$\text{s.t}: \ C(\tilde{\gamma}-\gamma) = 0 \tag{29}$$

A Lagrangian function is defined as follows to solve the above optimization problem

$$L(\tilde{\gamma}, \lambda) = J(\tilde{\gamma}) + \lambda^T C(\tilde{\gamma}-\gamma) \tag{30}$$

where $\lambda \in R^4$ is a vector of Lagrange multipliers. By calculating the partial derivative of equation (30), we have

$$\begin{cases} \partial_{\tilde{\gamma}} L(\tilde{\gamma}, \lambda) = -\beta\tau_{h-r}(t_i) + \frac{1}{\alpha u} Z^T Z(\tilde{\gamma}-\gamma) + C^T\lambda = 0 \\ \partial_{\lambda} L(\tilde{\gamma}, \lambda) = C(\tilde{\gamma}-\gamma) = 0 \end{cases} \tag{31}$$

By solving equation (31), we can obtain the following result

$$\tilde{\gamma} = \gamma + u\alpha W \beta \tau_{h-r}(t_i) \tag{32}$$

1083-4435 (c) 2020 IEEE. Personal use is permitted, but republication/redistribution requires IEEE permission. See http://www.ieee.org/publications_standards/publications/rights/index.html for more information.
Authorized licensed use limited to: Carleton University. Downloaded on May 27,2021 at 01:39:09 UTC from IEEE Xplore. Restrictions apply.

This article has been accepted for publication in a future issue of this journal, but has not been fully edited. Content may change prior to final publication. Citation information: DOI 10.1109/TMECH.2021.3053562, IEEE/ASME Transactions on Mechatronics

where

$$W = (I - (Z^T Z)^{-1} C^T (C(Z^T Z)^{-1} C^T)^{-1} C)(Z^T Z)^{-1}, I \in R^{N \times N} \quad (33)$$

where I is an identity matrix. The Hessel matrix is obtained as follow to ensure that the $\tilde{\gamma}$ in equation (32) minimizes the cost function $J(\tilde{\gamma})$ in equation (26).

$$\partial_{\tilde{\gamma}}(\partial_{\tilde{\gamma}}(J(\tilde{\gamma}))) = \frac{Z^T Z}{\alpha u} \quad (34)$$

As Z is a positive finite differencing matrix and $\alpha > 0, u > 0$, we can infer that $\tilde{\gamma}$ in equation (32) minimizes $J(\tilde{\gamma})$ in equation (26), subject to the equality constraints. We select the constant α as follows:

$$\alpha = \frac{\delta}{(p+\delta)\|W\|} \quad (35)$$

Thus, substituting equation (35) into (32), we can get the best vector field function, and the final equation of TDA as follows:

$$\begin{cases} \Gamma_d(u,t) = \tilde{\gamma} = \gamma + uV(t) = \Gamma_d(0,t) + uV(t), t \in [t_i, t_j] \\ V(t) = \delta H \tau_{h-r}(t_i) \\ H = \dfrac{W\beta}{(p+\delta)\|W\|} \end{cases} \quad (36)$$

REFERENCES

[1] T. Zhang, "Guidelines for stroke rehabilitation in China (2011 full version)," *Chin. J. Rehabil. Theory Pract.*, vol. 18, no. 4, pp. 301-318, Apr. 2012.

[2] M. Dam, P. Tonin, S. Casson, M. Ermani, G. Pizzolato, V. Iaia, and L. Battistin, "The effects of long-term rehabilitation therapy on poststroke hemiplegic patients," *Stroke*, vol. 24, no. 8, pp. 1186-1191, Apr. 1993.

[3] H. I. Krebs, N. Hogan, M. L. Aisen, and B. T. Volpe, "Robot-aided neurorehabilitation," *IEEE transactions on rehabilitation engineering*, vol. 6, no. 1, pp. 75-87, Mar. 1998.

[4] M. Ochi, F. Wada, S. Saeki, and K. Hachisuka, "Gait training in subacute non-ambulatory stroke patients using a full weight-bearing gait-assistance robot: A prospective, randomized, open, blinded-endpoint trial," *Journal of the neurological sciences*, vol. 353, no. 1-2, pp. 130-136, Jun. 2015.

[5] T. Nef, M. Mihelj, G. Kiefer, C. Perndl, R. Muller, and R. Riener, "ARM in exoskeleton for arm therapy in stroke patients," in *Proceedings IEEE 10th international conference on rehabilitation robotics*, Noordwijk, Netherlands, 2007, pp. 68–74.

[6] B. Chen *et al.*, "Recent developments and challenges of lower extremity exoskeletons," *Journal of Orthopaedic Translation*, vol. 5, pp. 26-37, Apr. 2016.

[7] G. Kwakkel, B. J. Kollen, and H. I. Krebs, "Effects of robot-assisted therapy on upper limb recovery after stroke: a systematic review," *Neurorehabilitation and Neural Repair*, vol. 22, no. 2, pp. 111–121, Sept. 2008.

[8] B. P. H. Chung, "Effectiveness of robotic-assisted gait training in stroke rehabilitation: A retrospective matched control study," *Hong Kong Physiotherapy Journal*, vol. 36, pp. 10-16, Jun. 2017.

[9] G. Colombo, M. Joerg, R. Schreier, and V. Dietz, "Treadmill training of paraplegic patients using a robotic orthosis," *Journal of rehabilitation research and development*, vol. 37, no. 6, pp. 693-700, Nov. 2000.

[10] Z. Warraich and J. A. Kleim, "Neural plasticity: The biological substrate for neurorehabilitation," *PM&R*, vol. 2, no. 12, pp. S208–S219, Dec. 2010.

[11] A. Duschau-Wicke, J. von Zitzewitz, A. Caprez, L. Lunenburger, and R. Riener, "Path control: a method for patient-cooperative robot-aided gait rehabilitation," *IEEE Transactions on Neural Systems and Rehabilitation Engineering*, vol. 18, no. 1, pp. 38-48, Oct. 2009.

[12] S. Hussain, P. K. Jamwal, M. H. Ghayesh, and S. Q. Xie, "Assist-as-needed control of an intrinsically compliant robotic gait training orthosis," *IEEE Transactions on Industrial Electronics*, vol. 64, no. 2, pp. 1675-1685, Jun. 2016.

[13] Z. Shen, J. Zhou, J. Gao, and R. Song, "Torque Tracking Impedance Control for a 3DOF Lower Limb Rehabilitation Robot," in *Proceedings International Conference on Advanced Robotics and Mechatronics (ICARM)*, Singapore, Singapore, 2018, pp. 294-299.

[14] P K. Jamwal, S, Hussain, M H. Ghayesh, S V. Rogozina, "Impedance control of an intrinsically compliant parallel ankle rehabilitation robot," *IEEE Transactions on Industrial Electronics*, vol. 63, no.6, pp. 3638-3647, Jan. 2016.

[15] Z. Shen, Y. Zhuang, J. Zhou, J. Gao, and R. Song, "Design and Test of Admittance Control with Inner Adaptive Robust Position Control for a Lower Limb Rehabilitation Robot ," *International Journal of Control, Automation and Systems*, vol.18, no. 1, pp.134-142, Jan. 2020.

[16] Y. Zhuang, S. Yao, C. Ma, and R. Song, "Admittance control based on EMG-driven musculoskeletal model improves the human–robot synchronization," *IEEE Transactions on Industrial Informatics*, vol. 15, no. 2, pp. 1211-1218. Feb. 2019.

[17] R. Riener, L. Lunenburger, S. Jezernik, M. Anderschitz, G. Colombo, and V. Dietz, "Patient-cooperative strategies for robot-aided treadmill training: first experimental results," *IEEE Transactions on Neural Systems and Rehabilitation Engineering*, vol. 13, no. 3, pp. 380-394, Sept. 2005.

[18] Y. Li, and S. S. Ge, "Human–robot collaboration based on motion intention estimation," *IEEE/ASME Transactions on Mechatronics*, vol. 19, no.3, pp. 1007-1014, Jun. 2013.

[19] A. Taherifar, G. Vossoughi, and A. Selk Ghafari, "Optimal target impedance selection of the robot interacting with human," *Advanced Robotics*, vol. 31, no. 8, pp. 428-440, Jan. 2017.

[20] F. Ferraguti, et al., "A variable admittance control strategy for stable physical human–robot interaction," *The International Journal of Robotics Research*, vol. 38, no. 6, pp.747-765, Apr. 2019.

[21] F. Dimeas and N. Aspragathos, "Online stability in human-robot cooperation with admittance control," *IEEE transactions on haptics*, vol. 9, no. 2, pp. 267-278, Jan. 2016.

[22] E. Guanziroli, et al., "Assistive powered exoskeleton for complete spinal cord injury: correlations between walking ability and exoskeleton control," *European journal of physical and rehabilitation medicine*, vol. 55, no. 2, pp. 209-216, Aug. 2019.

[23] A. Q. Keemink, H. van der Kooij, and A. H, Stienen, "Admittance control for physical human–robot interaction," *The International Journal of Robotics Research*, vol. 37, no. 11, pp.1421-1444, Apr. 2018

[24] P. D. Labrecque, and C. Gosselin, "Variable admittance for pHRI: from intuitive unilateral interaction to optimal bilateral force amplification," *Robotics and Computer-Integrated Manufacturing*, vol, 52, pp.1-8, Aug. 2018.

[25] M. Zhang, S. Q. Xie, X. Li, G. Zhu, W. Meng, X. Huang, and A. J. Veale, "Adaptive patient-cooperative control of a compliant ankle rehabilitation robot (CARR) with enhanced training safety," *IEEE Transactions on Industrial Electronics*, vol. 65, no. 2, pp. 1398-1407, Feb. 2018.

[26] C. Ott, R. Mukherjee, and Y. Nakamura, "Unified impedance and admittance control," in *Proceedings IEEE International Conference on Robotics and Automation*, Anchorage, Alaska, USA, 2010, pp. 554-561.

[27] Y. Aydin, O. Tokatli, V. Patoglu, and C. Basdogan, "Stable physical human-robot interaction using fractional order admittance control," *IEEE transactions on haptics*, vol. 11, no. 3, pp. 464-475, Sept. 2018.

[28] S. S. Ge, Y. Li, and C. Wang. "Impedance adaptation for optimal robot–environment interaction," *International Journal of Control*, vol. 87, no. 2, pp. 249-263, Jul. 2014.

[29] B. Kim, J. Park, S. Park, and S. Kang, "Impedance learning for robotic contact tasks using natural actor-critic algorithm," *IEEE Transactions on Systems, Man, and Cybernetics, Part B (Cybernetics)*, vol. 40, no. 2, pp. 433-443, Apr. 2009.

[30] D. P. Losey and M. K. O'Malley. "Trajectory deformations from physical human–robot interaction," *IEEE Trans. on Robotics*, vol. 34, no.1, pp. 126-138, Feb. 2018.

[31] J. F. Veneman, et al., "Design and evaluation of the LOPES exoskeleton robot for interactive gait rehabilitation," *IEEE Transactions on Neural Systems and Rehabilitation Engineering*, vol. 15, no. 3, pp. 379-386, Sept. 2007.

[32] Z. Li, B. Huang, Z. Ye, M. Deng, and C. Yang, "Physical Human–Robot Interaction of a Robotic Exoskeleton By Admittance Control," *IEEE Trans. on Industrial Electronics*, vol. 65, no. 12, pp. 9614-9624, Dec. 2018.

1083-4435 (c) 2020 IEEE. Personal use is permitted, but republication/redistribution requires IEEE permission. See http://www.ieee.org/publications_standards/publications/rights/index.html for more information.
Authorized licensed use limited to: Carleton University. Downloaded on May 27,2021 at 01:39:09 UTC from IEEE Xplore. Restrictions apply.

This article has been accepted for publication in a future issue of this journal, but has not been fully edited. Content may change prior to final publication. Citation information: DOI 10.1109/TMECH.2021.3053562, IEEE/ASME Transactions on Mechatronics

[33] N. Hogan. "Impedance control: An approach to manipulation: Part II—Implementation," Journal of dynamic systems, measurement, and control, vol. 107, no. 1, pp. 8-16, Mar. 1985.
[34] N. Hogan, and D. Sternad, "Sensitivity of smoothness measures to movement duration, amplitude, and arrests," *Journal of motor behavior*, vol. 41, no. 6, pp. 529-534, Nov. 2009.
[35] K. H. Lee, *et al*., "Enhanced Transparency for Physical Human-Robot Interaction Using Human Hand Impedance Compensation," *IEEE/ASME Transactions on Mechatronics*, vol. 23, no. 6, pp. 2662-2670, Dec. 2018.
[36] J. Wu, J. Gao, R. Song, R. Li, Y. Li, and L. Jiang, "The design and control of a 3DOF lower limb rehabilitation robot," *Mechatronics*, vol. 33, pp. 13-22, Feb. 2016.
[37] N. Hogan, "On the stability of manipulators performing contact tasks," *IEEE Journal on Robotics and Automation*, vol. 4, no. 6, pp.677-686, Dec. 1988.
[38] T. Tsumugiwa, Y. Fuchikami, A. Kamiyoshi, R. Yokogawa, and K. Yoshida, "Stability analysis for impedance control of robot in human-robot cooperative task system," *Journal of Advanced Mechanical Design, Systems, and Manufacturing*, vol.1 no. 1, pp.113-121, Mar. 2007.
[39] V. S. Chib, J. L. Patton, K. M. Lynch, et al. "Haptic identification of surfaces as fields of force," *Journal of neurophysiology*, vol. 95, no. 2, pp. 1068-1077, Feb. 2006.
[40] E. Burdet and T. E. Milner, "Quantization of human motions and learning of accurate movements," *Biological Cybernetics*, vol. 78, no. 4, pp. 307-318, May 1998.
[41] F. A. Mussa-Ivaldi, "Modular features of motor control and learning," *Current opinion in neurobiology*, vol. 9, no. 6, pp.713-717, Dec. 1999.
[42] B. Corteville, E. Aertbeliën, H. Bruyninckx, J. De Schutter, and H.Van Brussel, "Human-inspired robot assistant for fast point-to-point movements," in *Proceedings IEEE International Conference on Robotics and Automation*, Roma, Italy, 2007, pp. 3639-3644.
[43] H. Y. Li, et al., "Stable and compliant motion of physical human–robot interaction coupled with a moving environment using variable admittance and adaptive control," *IEEE Robotics and Automation Letters*, vol. 3, no. 3, pp. 2493-2500, Jul. 2018.
[44] H. S. Jørgensen, H. Nakayama, H. O. Raaschou, and T. S. Olsen, "Recovery of walking function in stroke patients: the copenhagen stroke study," *Archives of physical medicine and rehabilitation*, vol. 76, no.1, pp. 27-32, Aug. 1995.
[45] J. Park, "Movement disorders following cerebrovascular lesion in the basal ganglia circuit," *Journal of movement disorders*, vol. 9, no. 2, pp.71-79, May 2016.
[46] W Vattanasilp, L. Ada, and J. Crosbie, "Contribution of thixotropy, spasticity, and contracture to ankle stiffness after stroke," *Journal of Neurology, Neurosurgery & Psychiatry*, vol. 69, no. 1, pp. 34-39, Feb. *2000*.
[47] A. Ajoudani, N. G. Tsagarakis, and A. Bicchi, "Tele-impedance: Preliminary results on measuring and replicating human arm impedance in tele operated robots," in *Proceedings IEEE international conference on robotics and biomimetics*, Karon Beach, Phuket, Thailand, 2011, pp. 216-222.
[48] S. Yao, Y. Zhuang, Z. Li, and R. Song, "Adaptive admittance control for an ankle exoskeleton using an EMG-driven musculoskeletal model," *Frontiers in neurorobotics*, vol. 12, no. 16, pp. 1-12, Apr. 2018.

Jie Zhou received the B. Eng. degree in mechanical engineering from Jiangxi University of Science and Technology, Ganzhou, China, in 2015, the M.S. degree in Mechanical design and theory from Northeastern University, Shenyang, China, in 2018. He studied in the Laboratory of Space Automation Technology of Shenyang Institute of Automation Chinese Academy of Sciences from 2016 to 2017. He is now with Department of Biomedical Engineering, Sun Yat-Sen University, P. R. China, pursuing his Ph.D. degree.

His research interests include human-robot interaction, musculoskeletal modeling, robot-assisted stroke rehabilitation, and rehabilitation evaluation.

Zhijun Li (M'07-SM'09) received the Ph.D. degree in mechatronics, Shanghai Jiao Tong University, P.R. China, in 2002. From 2003 to 2005, he was a postdoctoral fellow in Department of Mechanical Engineering and Intelligent systems, The University of Electro-Communications, Tokyo, Japan. From 2005 to 2006, he was a research fellow in the Department of Electrical and Computer Engineering, National University of Singapore, and Nanyang Technological University, Singapore. From 2017, he is a Professor in Department of Automation, University of Science and Technology, Hefei, China. From 2019, he is the Vice Dean of School of Information Science and Technology, University of Science and Technology of China, China. His current research interests include service robotics, teleoperation systems, nonlinear control, and neural network optimization.

Dr. Li has been the Co-chairs of the Technical Committee on Bio-Mechatronics and Bio-Robotics Systems (B^2S), the IEEE Systems, Man and Cybernetics Society, the IEEE Technical Committee on Neuro-Robotics Systems, and the IEEE Robotics and Automation Society since 2016. He is an Editor-at-Large for the Journal of Intelligent and Robotic Systems, and an Associate Editor of several IEEE transactions. He has been the General Chair and Program Chair of 2016 and 2017 IEEE Conference on Advanced Robotics and Mechatronics, respectively.

Xianming Li received the B.S. degree in biomedical engineering from Sun Yat-sen University, Guangzhou, China in 2018, where he is currently working toward the M.S. degree in biomedical engineering. His research interests include robot-assisted stroke rehabilitation, human-robot interaction, biomedical signal processing, and rehabilitation evaluation.

Xiaoyun Wang received the PhD degree from Department of Rehabilitation Sciences, the Hong Kong Polytechnic University. She is now working as an associate investigator in Guangdong Work Injury Rehabilitation Center. Her research focused on effect and mechanism of physical intervention, such as ultrasound, vibration and so on, on bone healing.

Rong Song received the B. Eng. degree in electrical engineering from Tsinghua University in 1999, the M.S. degree in electronic engineering from Shantou University in 2002, and the Ph.D. degree in biomedical engineering from Hong Kong Polytechnic University in 2006. He is currently a Professor with the School of Biomedical Engineering, Sun Yat-sen University, China.

His research interests include musculoskeletal modeling, biomedical signal processing, human motion analysis, and robot-assisted stroke rehabilitation, human-robot interaction, biomedical signal processing, and rehabilitation evaluation.

1083-4435 (c) 2020 IEEE. Personal use is permitted, but republication/redistribution requires IEEE permission. See http://www.ieee.org/publications_standards/publications/rights/index.html for more information.
Authorized licensed use limited to: Carleton University. Downloaded on May 27,2021 at 01:39:09 UTC from IEEE Xplore. Restrictions apply.